RSC Advances

PAPER

Probing the 2D-to-3D structural transition in gold clusters with a single sulfur atom: $Au_xS^{0,\pm1}$ ($x = 1$–10)

Cite this: *RSC Adv.*, 2014, **4**, 15066

Hui Wen,[ab] Yi-Rong Liu,[b] Kang-Ming Xu,[b] Teng Huang,[b] Chang-Jin Hu,[b] Wei-Jun Zhang[abc] and Wei Huang*[abc]

Received 21st December 2013
Accepted 10th March 2014

DOI: 10.1039/c3ra47873d

www.rsc.org/advances

Gold sulfur clusters have received much attention because of the dramatic effect that the gold–sulfide interaction produces in thiol-passivated gold nanoparticles. We present a systematic theoretical study of the electronic properties and geometric structures of $Au_xS^{0,\pm1}$ ($x = 1$–10) clusters using the basin-hopping global optimization technique coupled with density functional theory (DFT-BH) methods. Higher-level *ab initio* calculations are performed to aid in structural assignment. The same species with different electric charges possess different configurations. The 2D-to-3D structural transitions of the global minimum structures of cationic, neutral, and anionic Au_xS clusters are found at the sizes of $x = 3$, 6, and 9, respectively. It is found that the Au_5S cluster can be regarded as the building-block unit for the evolution of larger Au–S clusters. The tendency toward planarity of each Au–S cluster species, which is similar to that of bare Au clusters, may be attributed to the strong relativistic effects of Au and the similar electronegativity between Au and S. The trends of the binding energies, electron affinities, and bond parameters with increasing cluster size are studied in detail for each species. The results demonstrate that the binding energies and second-order differences exhibit interesting oscillatory behaviors; it is believed that anionic clusters may be the most suitable for catalysis.

1. Introduction

Small atomic clusters are considered to be well-defined model systems that exhibit specific properties. Size-selected gold clusters have attracted significant attention because of their wide use in medicine,[1,2] catalysis,[3–9] and non-linear optical devices.[10,11] Model studies have shown that low dimensionality may be important for supported gold catalysts.[12] High-resolution electron microscopy has also revealed that small gold clusters containing one or two atomic layers are the active species for catalysis.[13,14] Thus, understanding the properties of the selected sizes and the 2D-to-3D structural transition is of critical importance.

Many groups have studied the critical size of the 2D-to-3D structural transition of pure Au clusters.[15–20] Häkkinen and Landman studied neutral and anionic gold clusters and found that they are planar when $n < 8$ and $n < 7$, respectively.[20] Furthermore, they predicted that anionic clusters will undergo a structural transition from $n = 9$ onward. However, subsequent experiments reaffirmed that the 2D-to-3D transition does occur at Au_{12}^- using ion-mobility,[19] trapped ion electron diffraction,[16] and Ar-tagging[15] measurements.

Doping heteroatoms into gold clusters can have a significant effect on the geometries and stabilities of the clusters. The study of sulfur-doped gold clusters has received much attention and is motivated in part by understanding the Au–S interactions, which are important in thiol-passivated gold nanoparticles. Sulfur has also been used as a surfactant and identified as the most suitable atom to act as a clip atom between molecular devices and gold electrodes.[7,21–23] Sulfur–gold serves as a nice example of a semiconductor with an intermediate band gap and mixed ionic bonding characteristics.[24,25] The interactions between thiolate-ligands and gold are very important in self-assembled monolayers (SAMs) and ligand-protected gold nanoparticles.[26–34] Apart from the importance of Au–S interactions in the field of nanoelectronics, another interesting aspect of Au–S interactions is the small difference between their electronegativity, the values of Au and S are 2.54 and 2.58, respectively, despite the fact that Au is a metal, while S is a nonmetal.

The importance of the 2D-to-3D structural transition of pure gold clusters has stimulated studies of the interaction of gold clusters with a single sulfur atom and studies aimed at understanding the differences between bare Au clusters and Au_xS clusters. Majumder[35] employed *ab initio* molecular dynamics simulations to investigate the structures and electronic

[a]*Key Laboratory of the Atmospheric Composition and Optical Radiation, Chinese Academy of Sciences, Hefei, Anhui 230031, China. E-mail: Huangwei6@ustc.edu.cn*
[b]*Laboratory of Atmospheric Physico-Chemistry, Anhui Institute of Optics & Fine Mechanics, Chinese Academy of Sciences, Hefei, Anhui 230031, China*
[c]*School of Environmental Science & Optoelectronic Technology, University of Science and Technology of China, Hefei, Anhui 230026, China*

properties of neutral Au_n clusters and their interactions with a single S atom. Woldeghebriel *et al.*[2] studied the response of cationic gold clusters to a single sulfur atom and found that the cationic species prefer the 3D configuration. Our recent work[36] revealed the 1D-to-2D structural transition at $x = 4$ of Au_xS^- ($x = 2$–5), and strong covalent bonding between S and Au was also found. It is noteworthy that Becke's three-parameter hybrid exchange functional with Lee, Yang, and Parr (B3LYP) theory yields results that are highly consistent with those of photoelectron spectroscopy (PES).

Because neutral and cationic clusters cannot be studied using PES, theoretical studies become more crucial for these systems. To obtain a systematic insight into the doping of gold clusters with a single sulfur atom, in this work, the $Au_xS^{0,\pm1}$ ($x = 1$–10) systems are thoroughly studied based on the same method used in our recent work[36] and compared to other available theoretical results. The goal of this work is to provide effective guidelines for future experimental studies and contribute further understanding of the structures and electronic properties of Au–S clusters, which may be useful in creating a new type of Au–S nanostructure for nanocatalysis.

2. Computational methods

We carried out extensive and unbiased searches for the global minimum structures of $Au_xS^{0,\pm1}$ ($x = 1$–10) using the basin-hopping (BH, a stochastic algorithm which attempts to find the global minimum of a smooth scalar function of one or more variables[70]) global optimization method coupled with the first-principles generalized gradient approximation DFT method.[37–42] To generate the isomer populations in the initial BH searches, the gradient-corrected Perdew–Burke–Ernzerhof (PBE)[43] exchange–correlation functional and the double-numerical polarized (DNP) basis set with effective core potentials (ECPs) were used with a medium-level convergence criterion, as implemented in the Dmol^3 code.[44] More than 200 structures were sampled, and the isomers were ranked according to their relative energies for further optimization at higher levels.

The top twenty low-lying isomers in each case were further optimized using PBE/CRENBL ECP theory, the small core potential due to Christiansen, Ross, Ermler, Nash, Bursten, and large-valence-shape-consistent,[69] which has been proven to be suitable for the Au atom.[40,45,46] For the S atom, we examined the B3LYP,[47,48] PBE and B2PLYPD[71] (which is B2PLYP functional with "D2" dispersion corrections) functionals together with the aug-cc-pVDZ basis set[49] and the 6-311++G** basis set[50] for optimization, while the aug-cc-pVTZ basis set[49] and the 6-311++G(3df,3pd) basis set[50] were used for the second round of optimization, as implemented in the NWCHEM 6.1 software package.[51]

Single-point energy calculations were performed with the inclusion of the spin-orbit effect (SO) for anionic Au_xS^-. Our previous studies[37–42] proved that the inclusion of SO can produce quantitative simulated PES results. Harmonic vibrational frequencies were calculated to confirm whether the lowest-energy isomers are true minima. All the calculations are spin-restricted for closed-shell molecules and spin-unrestricted for open-shell species. Higher-level *ab initio* calculations were also performed to aid in structural assignments. In order to contain the relativistic effects in these calculations, the Stuttgart/Dresden effective core potential (SDD) has been employed. The SDD basis set was augmented by the polarizations functions on all atoms.[52,53] For comparison, the aug-cc-pVTZ basis set for S and cc-pVTZ-pp basis set for Au were also used to calculate the single point energy under the MP2 level of theory.

3. Results and discussions

To test the performance of the computational methods employed in the present investigation, it is important to compare the results to those of previously published studies.[2,31,35,54,55] In this section, we will present the low-lying structures obtained during an exhaustive search and discuss the structural details of a few top-ranked isomers of $Au_xS^{0,\pm1}$ ($x = 1$–10) clusters, as shown in Figs. 1, 3 and 4 and Tables 1 and 2.

3.1. Equilibrium geometries

A. Anionic Au_xS^- ($x = 2$–10) clusters. A combined negative-ion photoelectron spectroscopic and theoretical investigation of Au_xS^- ($x = 2$–5) was recently conducted by our group.[36] Briefly, Au_2S^- was found to have an asymmetric linear structure (S–Au–Au). Au_3S^- has a planar rhombus structure with C_{2v} symmetry. Two isomers were experimentally observed to co-exist for Au_4S^-, a quasi-1D bent structure (C_{2v}) and a 2D planar (C_s) low-lying isomer; the two structures are similar in energy. The global minimum of Au_5S^- was found to be a highly stable planar triangular structure. Thus, a 1D-to-2D structural transition is observed in Au_xS^- clusters at $x = 4$.

We employed several theoretical methods to investigate the structures of larger Au_xS^- ($x = 6$–10) clusters, and the relative energies of selected low-lying isomers obtained using various methods are summarized in Table 1. In most cases, the energy rankings obtained using B2PLYPD are in agreement with those obtained using other DFT methods without dispersion correction and the MP2 level of theory, except for the Au_6S^- clusters. The energy ordering of isomers b and c for Au_6S^- cluster are changed, but all the global minima for the anionic Au–S clusters obtained using B2PLYPD are great agreement with those obtained at other employed methods. The low-lying structures of larger Au_xS^- ($x = 6$–10) clusters obtained using B3LYP/6-311++G(3df,3pd) theory are shown in Fig. 1. For the Au_6S^- cluster, the lowest-energy isomer is found to be a planar structure. The isomers 6a and 6c (C_s symmetry and C_{2v} symmetry) are close in energy; isomer 6c is similar to the lowest-energy isomer of the bare Au_7^- cluster,[42,56–58] and we also found the dangling Au atom structure (Fig. 1 and 6d) presented in a previous report,[42] which consists of a triangular Au_5S^- unit with a terminal Au atom. The wheel hexagon shape with D_{2h} symmetry (Fig. 1 and 6f) is similar to that of the Au_7^+ cluster[19] but is much higher in energy (~0.86 eV). All calculations indicate that the global minimum of Au_7S^- favors a 2D planar structure (D_{2h} symmetry). Another isomer possesses C_s symmetry (Fig. 1 and 7e) with a relative energy of 0.3–0.6 eV, as calculated using various methods, which is similar to that of bare Au_8^-.[56]

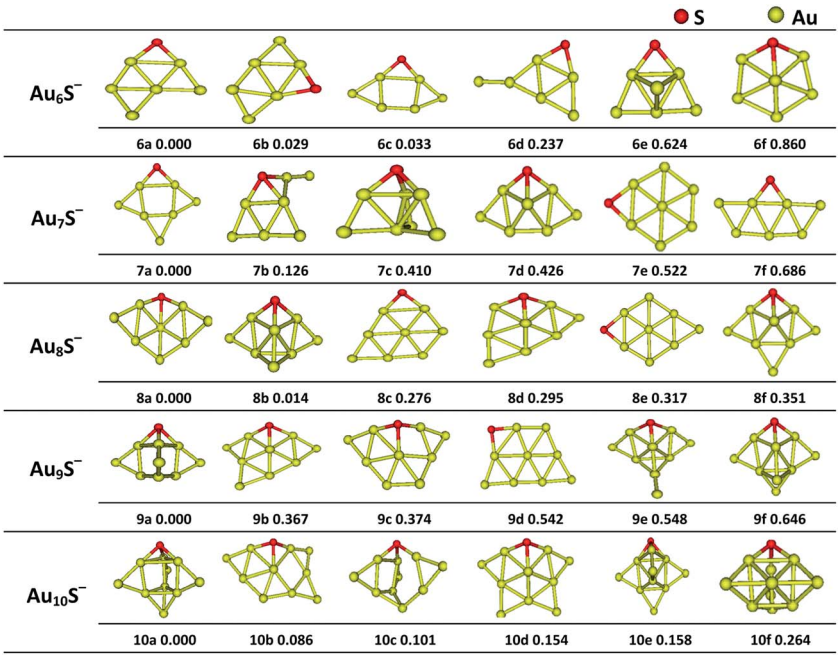

Fig. 1 Atomic structures of the lowest-energy structures and some of the low-lying isomers of Au_xS^- ($x = 2$–10) anionic clusters obtained using B3LYP/6-311++G(3df,3pd) theory. The energy of each isomer is given in eV. The yellow and red balls represent Au and S atoms, respectively.

Table 1 Relative energies and vertical detachment energies (VDEs) of top low-lying isomers of Au_xS^-, ($x = 6$–10) obtained using PBE/CRENBL ECP (PBE), PBE0/aug-cc-pVTZ (PBE0), PBE/aug-cc-pVTZ (PBE-a), PBE0/6-311++G(3df,3pd) (PBE0-6), B3LYP/6-311++G(3df,3pd) (B3LYP), B2PLYPD/aug-cc-pVTZ (B2PLYPD), and MP2/aug-cc-pVTZ (MP2) theory[a] (in eV)

		Relative energies							VDEs
Species	Isomers	PBE	PBE0	PBE-a	PBE0-6	B3LYP	B2PLYPD	MP2	B3LYP
Au_6S^-	a	**0.000**	**0.000**	**0.000**	**0.000**	**0.000**	**0.000**	**0.000**	3.426
	b	0.029	**0.000**			0.029	0.331	0.110	3.580
	c	0.033	0.469	0.027	0.024	0.033	0.164	0.206	3.769
Au_7S^-	a	**0.000**	**0.000**	**0.000**	**0.000**	**0.000**	**0.000**	**0.000**	3.468
	b	0.286	0.255	0.199	0.168	0.126	0.243	0.644	4.388
	c	0.207	0.263	0.241	0.216	0.410	0.374	0.022	4.186
Au_8S^-	a	**0.000**	**0.000**	**0.000**	0.001	**0.000**	**0.000**	0.192	3.125
	b	0.055	0.005	0.035	**0.000**	0.014	0.086	**0.000**	3.016
	c	0.268	0.337	0.35	0.337	0.276	0.377	0.421	4.007
Au_9S^-	a	**0.000**		**0.000**	**0.000**	**0.000**	**0.000**	**0.000**	4.487
	b	0.275		0.334	0.332	0.367	0.297	0.364	3.987
	c	0.425		0.407	0.407	0.374	0.501	0.397	4.001
$Au_{10}S^-$	a			**0.000**		**0.000**	**0.000**	**0.000**	2.775
	b			0.237		0.086	0.184	0.797	3.276
	c			0.26		0.101	0.558	0.902	3.399

[a] Isomers are ranked according to their relative energies obtained using B3LYP/6-311++G(3df,3pd) theory. The VDEs were computed using B3LYP/6-311++G(3df,3pd) theory. The vertical detachment energies were determined as follows: VDE = E(neutral at anion equilibrium geometry) − E(optimized anion). The energies of the lowest-energy isomers are highlighted in bold.

Unlike the case of small Au_xS^- ($x \leq 7$) clusters, for Au_8S^-, 2D and 3D structures are nearly isoenergetic using the employed DFT methods and therefore become competitive. Higher-level *ab initio* calculations (MP2/aug-cc-pVTZ) were performed to aid in structural assignment, and it was found that the relative energy of the 3D structure is slightly lower than that of the planar one. Indeed, the appearance of a 3D configuration as the lowest-energy structure begins at Au_9S^-. For Au_9S^-, all calculations predict that the isomer 9a (Fig. 1), which contains Au_6S^- (Fig. 1 and 6d) units, is the global minimum. The lowest-energy structure for the $Au_{10}S^-$ cluster also possesses a 3D configuration, which consists of three minimum Au_7S^- (D_{2h} symmetry) units, according to the employed methods.

According to our previous study,[36] it is remarkable that the simulated spectra obtained using B3LYP/6-311++G(3df,3pd)//B3LYP/6-311++G** theory for the S atom and PBE0/CRENBL

Table 2 Relative energies and the vertical electron affinities (EA_{vert}) of top low-lying isomers of neutral Au_xS and corresponding cationic Au_xS^+, (x = 2–10) clusters obtained using PBE/aug-cc-pVTZ (PBE), B3LYP/6-311++G(3df,3pd) (B3LYP), B2PLYPD/aug-cc-pVTZ (B2PLYPD) and MP2/aug-cc-pVTZ (MP2) theory[a] (in eV)

Neutral species	Isomers	Relative energies				EA_{vert}	Cationic species	Isomers	Relative energies			
		PBE	B3LYP	B2PLYPD	MP2	B3LYP			PBE	B3LYP	B2PLYPD	MP2
Au_2S	a	**0.000**	**0.000**	**0.000**	**0.000**	1.792	Au_2S^+	a	**0.000**	**0.000**	**0.000**	**0.000**
	b	3.372	1.868	1.576	3.090			b	3.423	0.804	0.423	0.044
Au_3S	a	**0.000**	**0.000**	**0.000**	0.098	3.307	Au_3S^+	a	**0.000**	**0.000**	**0.000**	**0.000**
	b	0.016	0.147	0.038	**0.000**	2.772		b		2.292	2.591	2.216
	c	0.237	0.262	0.277	0.425	2.227		c				
Au_4S	a	**0.000**	**0.000**	**0.000**	**0.000**	2.592	Au_4S^+	a		**0.000**	**0.000**	0.103
	b	0.062	0.018	0.142	0.390	2.767		b	**0.000**	0.237	0.388	**0.000**
	c	0.169	0.130	0.156		2.639		c	0.092	0.430	0.673	0.182
Au_5S	a		**0.000**	**0.000**	**0.000**	3.296	Au_5S^+	a	**0.000**	**0.000**	**0.000**	**0.000**
	b	**0.000**	0.220	0.105	1.231	2.640		b	0.114	0.146	0.323	0.002
	c	0.055	0.343	0.265		3.103		c		0.726		0.889
Au_6S	a	**0.000**	**0.000**	**0.000**	**0.000**	2.255	Au_6S^+	a	0.600	**0.000**	**0.000**	**0.000**
	b	0.347	0.409	0.354	0.376	2.675		b	0.247	0.093	0.107	0.244
	c	0.392	0.580	0.596	0.404	2.145		c	**0.000**	0.115	0.189	0.430
Au_7S	a	**0.000**	**0.000**	**0.000**	**0.000**	3.189	Au_7S^+	a	0.134	**0.000**	0.084	0.279
	b	0.315	0.547	0.218	0.086	3.287		b	**0.000**	0.071	**0.000**	**0.000**
	c	0.347	0.625	0.474	0.105	3.183		c		0.157	0.325	0.545
Au_8S	a	**0.000**	**0.000**	**0.000**	**0.000**	2.421	Au_8S^+	a	**0.000**	**0.000**	**0.000**	**0.000**
	b	0.311	0.195	0.536	0.965	2.402		b	0.153	0.013	0.327	0.605
	c	0.371	0.626	0.376	0.139	2.186		c	0.458	0.173	0.385	0.101
Au_9S	a	**0.000**	**0.000**	**0.000**	**0.000**	2.768	Au_9S^+	a	**0.000**	**0.000**	**0.000**	**0.000**
	b	0.475	0.070	0.224	0.141			b		0.454	0.328	0.276
	c	0.413	0.081	0.253		3.464		c	0.803	0.470	0.554	0.428
$Au_{10}S$	a		**0.000**	**0.000**	**0.000**	2.566	$Au_{10}S^+$	a	**0.000**	**0.000**	**0.000**	**0.000**
	b		0.318	0.454	0.542	2.539		b	0.036	0.027	0.109	0.207
	c		0.365			2.592		c	0.104	0.124	0.343	0.926

[a] Isomers are ranked according to their relative energies obtained using B3LYP/6-311++G(3df,3pd) theory. The EA_{vert} values were computed using B3LYP/6-311++G(3df,3pd) theory. The vertical electron affinities were determined as follows: EA_{vert} = E(optimized neutral) − E(anion at neutral equilibrium geometry). The energies of the lowest-energy isomers are highlighted in bold.

ECP (SO)//PBE/CRENBL ECP for the Au atom can yield results that are highly consistent with the experimental PES spectra (Fig. 2). The simulated PES spectra of the global minima and low-lying isomers of Au_xS^- (x = 6–10) using the same method mentioned above are shown in Fig. 3. The calculated vertical detachment energies (VDEs) are summarized in Table 1. The binding energies of deeper orbitals were then added to the first VDE to find VDEs for the excited states. The simulated spectra were obtained by fitting the computed VDEs with Gaussian functions of 0.04 eV widths. The simulated spectra well reproduce the experimental spectra for Au_xS^- (x = 2–5), especially for the Au_4S^- cluster (Fig. 2). The global minimum bent structure yields much higher VDEs, and its simulated spectrum is in good agreement with the main features observed experimentally. In contrast, the VDEs calculated for the low-lying planar isomer are much lower, and its simulated spectrum agrees well with the weaker low-binding-energy features observed experimentally.

B. Neutral Au_xS (x = 2–10) clusters. To study the charge-induced changes in the structures and electronic properties of the anionic clusters, we investigated the lowest and the low-lying configurations of neutral Au–S clusters. The top low-lying geometries of Au_xS clusters obtained using B3LYP/6-311++G(3df,3pd) theory are shown in Fig. 4, and the relative energies and the vertical electron affinities (EA_{vert}) for selected isomers are summarized in Table 2. The energy rankings obtained using DFT methods and also the B2PLYPD with dispersion correction are in agreement with those obtained using the high-accuracy MP2/aug-cc-pVTZ theory.

The optimized structure of Au_2S is found to have a bent Au–S–Au form using the three employed methods, and it forms an open Au–S–Au triangle with an angle of 89.32° according to the PBE/aug-cc-pVTZ theory. The highly stable bent Au_2S (C_{2v}) cluster can be seen as analogous to the H_2S (C_{2v}) molecule, demonstrating that Au mimics H in its bonding to sulfur. The Au/H analogy has been observed previously in Si–Au[59–61] and B–Au[62,63] clusters. Au_3S also has a bent structure with an Au–S–Au–Au connectivity according to both B3LYP/6-311++G(3df,3pd) and PBE/aug-cc-pVTZ theory. However, the MP2/aug-cc-pVTZ theory indicates that the planar rhombus structure, in which the sulfur atom is edge-capped with two gold atoms, is 0.098 eV lower in energy than the bent structure. We also confirmed the accuracy of the MP2/aug-cc-pVTZ result using the CCSD(T) theory. Generally, it is presumed that higher-level calculations yield more accurate results because of the limitations of DFT theory.

The ground-state geometry of Au_4S possesses a 2D planar configuration, in which the sulfur atom caps one side of the rhombus formed by the bare Au_4 cluster.[16,56] This result is in

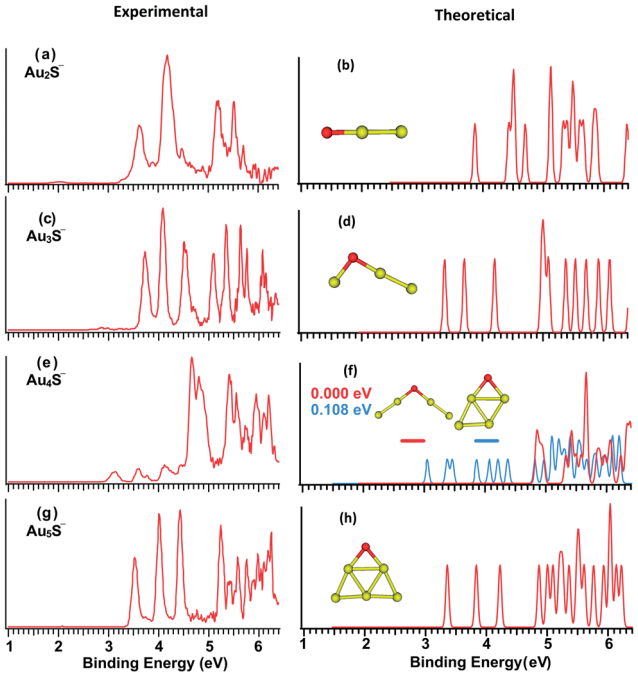

Fig. 2 Experimental (left panel) and simulated (right panel) photoelectron spectra for the global minima of Au_xS^- (x = 2–5) clusters, simulated photoelectron spectra were obtained under B3LYP/6-311++G(3df,3pd)//B3LYP/6-31++G** level of theory. The insets show the corresponding structures.

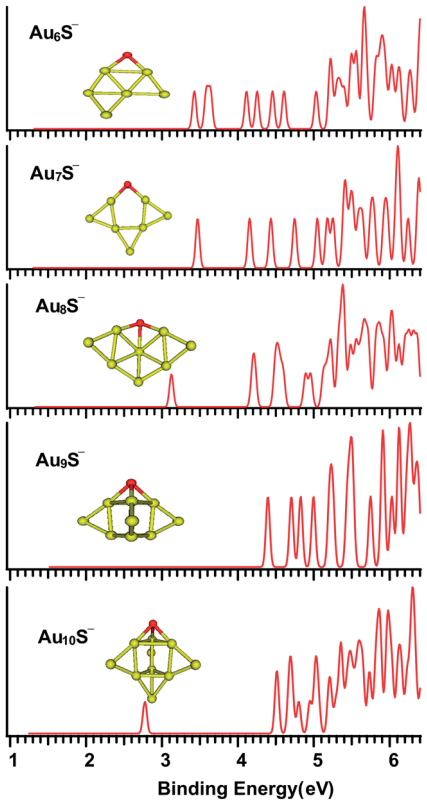

Fig. 3 Simulated photoelectron spectra for the global minima of Au_xS^- (x = 6–10) clusters using B3LYP/6-311++G(3df,3pd)//B3LYP/6-31++G** theory. The insets show the corresponding structures.

agreement with Majumder's work,[35] while Pérez *et al.*[64] found that the 3D isomer was the lowest-energy isomer. Other isomers of higher energies, including 3D atomic configurations, are listed in Fig. 4. The Au_5S cluster favors planar stacked triangles, and it is similar to its corresponding anionic cluster, in which the S atom is located at the apex position with two-fold coordination. The isomer with the next-higher energy, which has a 3D configuration in which the additional Au is bound to the S atom and remains outside of the planar structure of Au_4S or Au_4S^- clusters, is 0.220 eV higher in energy than the lowest structure.[35] The appearance of 3D geometries as the lowest-energy structures begins at Au_6S. The lowest-energy isomer with C_s symmetry can be identified as one gold atom adjoined on the minimum structure of an Au_5S unit (stacked triangular), as shown in Fig. 4 and 6a. The wheel structure (Fig. 4 and 6f) is similar to that of Au_7 cluster[20] and is considerably higher in energy (~1.008 eV) than the global minimum.

The Au_7S cluster exhibits a 3D configuration as the lowest-energy isomer, and it can be viewed as an Au_5S unit (stacked triangles) adjoined with a planar (C_s) Au_4S unit, sharing one S atom and two Au atoms in common, as shown in Fig. 4 and 7a. The structures of isomers 7e and 7f have also been found to correspond to the low-lying isomers of the bare Au_8^- cluster,[65] but both these isomers lie at higher energies than the global minimum according to all employed calculation methods. Based on the configuration of the Au_7S cluster, the minimum structure of the Au_8S cluster can be obtained by capping the triangular faces of the Au_4S cluster with an additional Au atom. The same growth pattern is observed for the Au_9S cluster, and the most stable configuration is a trihedral pyramid with three layers formed of Au_5S units. Therefore, considering the structural transition, we may refer to the Au_5S cluster as the building-block unit for the evolution of larger Au_xS clusters. However, the lowest-energy isomer of the $Au_{10}S$ cluster is formed of three D_{4h} symmetry units, which is similar to that of $Au_{10}S^-$. The vertical electron affinities (EA_{vert}) of selected isomers of each neutral species are quite close in energy.

C. Cationic Au_xS^+ (x = 2–10) clusters. To provide an understanding of the structures of the whole family of Au–S clusters, the cationic clusters were also thoroughly studied. The low-lying structures of Au_xS^+ (x = 2–10) clusters obtained using B3LYP/6-311++G(3df,3pd) theory are depicted in Fig. 5. The relative energies of Au_xS^+ obtained using various methods are summarized in Table 2. The Au_2S^+ cluster also favors a symmetric bent structure with an Au–S–Au bond angle of 98.79°, which is larger than the angle of the corresponding neutral cluster. The closed triangle shape with an acute bond angle is higher in energy. Au_3S^+ is found to be a 3D structure that possesses D_{3h} symmetry according to several theoretical methods, including the MP2/aug-cc-pVTZ theory, which is quite different from the structures of the Au_3S^- and Au_3S clusters. The isomer with the next higher energy is found to possess a planar "Y" shape (C_{2v}), which is consistent with a previous study. However, Woldeghebriel[2] reported that the lowest-energy

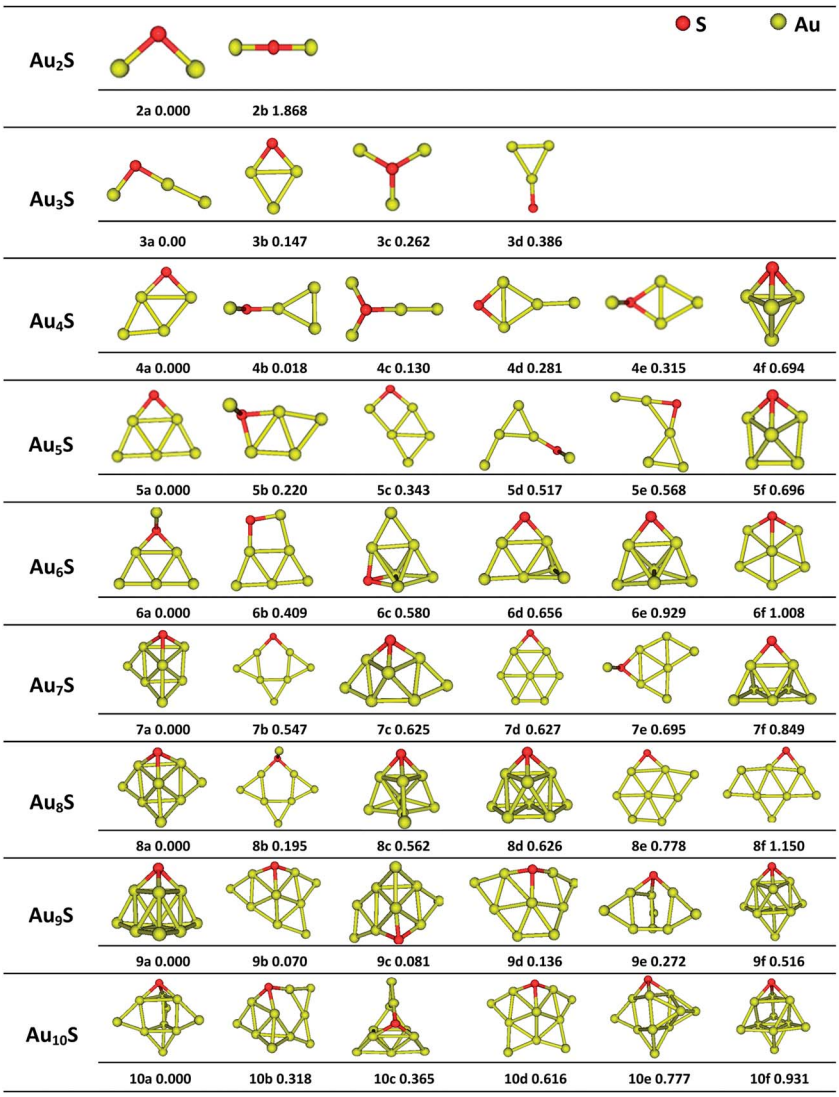

Fig. 4 Atomic structures of the lowest-energy structures and some of the low-lying isomers of neutral Au_xS ($x = 2$–10) clusters obtained using B3LYP/6-311++G(3df,3pd) theory. The energy of each isomer is given in eV. The yellow and red balls represent Au and S atoms, respectively.

structure of Au_3S^+ is another 3D structure configuration with all three Au atoms bonded together to form a triangle, and the isomer with the next-higher-energy to be planar with a kite-like quadrilateral structure using the LDA and GGA functionals. During the unbiased BH searches, we did obtain several initial structures, including the structures mentioned above;[2] however, all initial structures were converted to the lowest isomer in Fig. 5 when optimizing using the B3LYP/6-311++G(3df,3pd) theory.

All employed methods predicted that the minimum structure of the Au_4S^+ cluster possesses a 3D configuration. However, the isomer with an extra Au atom bonded to the S atom of the 2D planar rhombus while remaining outside of this plane (Fig. 5 and 4b) is found to be the global minimum using the MP2/aug-cc-pVTZ theory, but it is merely a low-lying isomer according to the B3LYP/6-311++G(3df,3pd) theory. The higher-symmetry structure with a diamond shape (Fig. 5 and 4c) is much higher in energy. The most stable isomer of the Au_5S^+ cluster is similar to the isomer 5b of Au_5S depicted in Fig. 4, but it is quite different from the corresponding neutral and anionic clusters.

In the lowest-energy structure of Au_6S^+, the additional Au atom joins the triangle-shaped gold trimer in the structure of the neutral Au_5S (Fig. 5 and 6a). The S atom remains in its position, and the remaining Au is seen to be out of the plane. The global minimum structure of Au_7S^+ is similar to that of the Au_7S cluster, and the next-higher-energy isomer according to the B3LYP/6-311++G(3df,3pd) theory can be viewed as another Au atom attached to the lowest-energy isomer of neutral Au_6S (6a), as shown in Fig. 4. Compared to the neutral Au_xS clusters, a similar structural evolution is also observed in the larger Au_xS^+ ($x = 8$–10) clusters. The structures of the cationic clusters are similar to those of the corresponding neutral and anionic clusters. The stacked-triangles shape is also a building-block unit in the lowest-energy structures observed for the Au_xS^+ ($x = 6$–9) clusters.

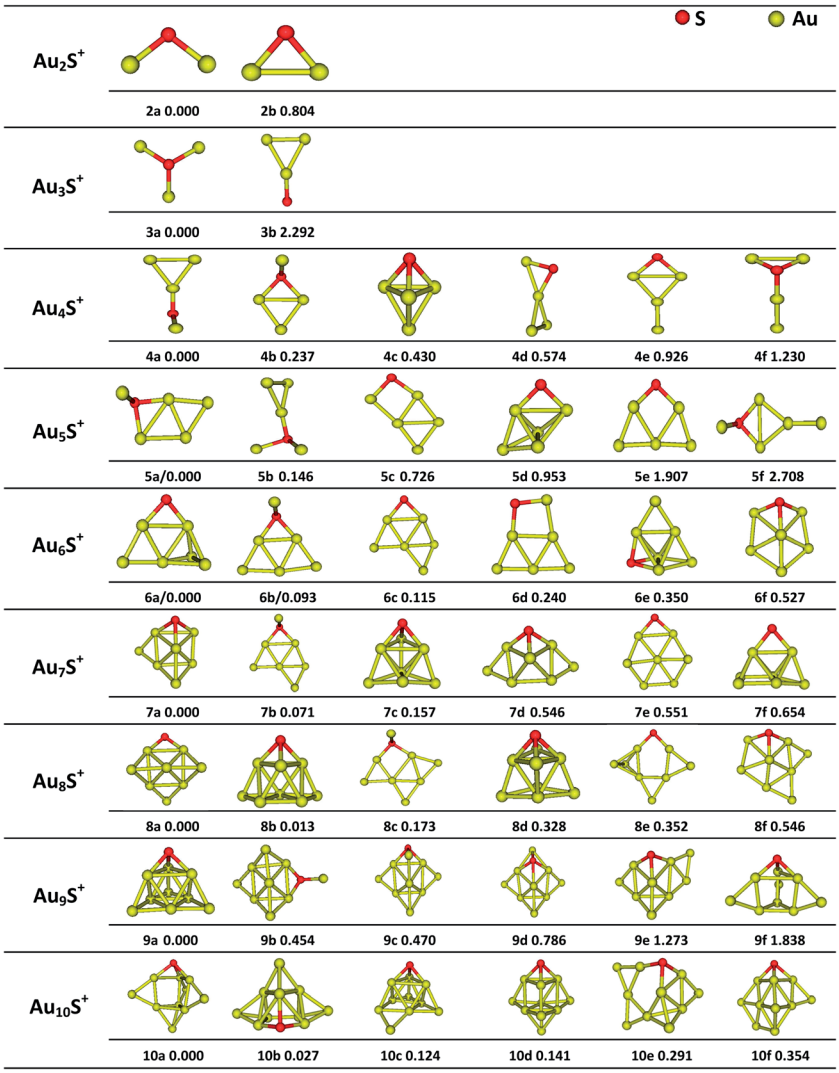

Fig. 5 Atomic structures of the lowest-energy structures and some of the low-lying isomers of cationic Au_xS^+ ($x = 2$–10) clusters obtained using B3LYP/6-311++G(3df,3pd) theory. The energy of each isomer is given in eV. The yellow and red balls represent Au and S atoms, respectively.

3.2. 2D-to-3D structural transition point

The calculations of the interactions of a sulfur atom with gold clusters are quite different from those of pure Au atom clusters. The lowest-energy isomers of each species according to the MP2/aug-cc-pVTZ theory are shown in Fig. 6. Both anionic and cationic clusters have closed-shell structures for the odd numbers of Au atoms. For $Au_xS^{0,\pm1}$ clusters, the planar rhombus structure and the stacked-triangles structure are observed to behave as two stable building blocks for most of larger structures. It should be noted that the Au_xS^+ clusters favor 3D configurations. Au_3S^+ is found to be the smallest possible 3D structure, which is in outstanding agreement with previous work.[2] Different dopant atoms can significantly alter the geometrical and electronic properties of the clusters. Recent theoretical work[66] regarding Au_nBe^+ clusters has indicated that a transition point from 2D to 3D structures occurs at $n = 6$.

For the minima of neutral Au–S clusters, the largest planar structure is observed for $x = 5$, which is in excellent agreement with Majumder's[35,54] findings, while Pérez *et al.*[64] reported that the 3D configuration first appeared for the Au_4S cluster. Compared with some metal atoms, such as Na and Mg,[54] sulfur atoms prefer two-fold coordination sites instead of four-fold coordination sites; these preferences reflect the structures of covalent and metallic bonds, respectively. Previous studies[36,67] have observed strong covalent bonding between S and Au, which may suggest that for the covalent bond, the electrons align along the bond axis, and the delocalization of the electrons leads to the structural planarity of the Au_5S cluster.

As we can see in Fig. 6, 2D-to-3D crossover occurs at a size of $x = 8$ for Au_xS^-, while for the same period element Al,[68] the 2D-to-3D transition of anionic Au–Al clusters is observed at $n = 5$. The preference of pure gold clusters for a 2D planar structure is attributed to the existence of strong relativistic effects, which enhances the s–d hybridization by shrinking the size of the 6s orbital with respect to the fully occupied $5d_z^2$ orbital.[15] As for the anionic Au–S clusters, the gold atom replaced by the S atom may

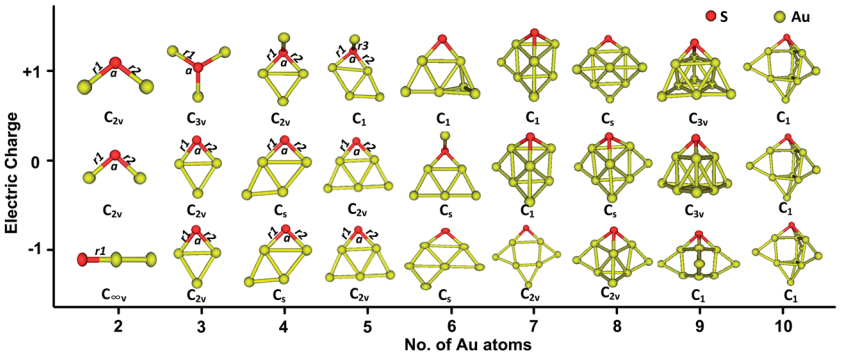

Fig. 6 The lowest-energy isomers of Au_xS ($x = 2$–10) species for various electric charges. All structures were obtained using MP2/aug-cc-pVTZ theory. The yellow and red balls represent Au and S atoms, respectively.

be attributed to their similar electronegativity, which form the planar structures.

It is known that small gold clusters that contain one or two atomic layers can be used as active species for catalysis.[13,14] Assuming that the planar structure is more active than the 3D configuration, the anionic clusters may therefore be the best candidate species for nanocatalysis.

3.3. Bonding parameters of $Au_xS^{0,\pm1}$

The bonding parameters ($r1$, $r2$, $r3$, and a) of the lowest-energy isomers of $Au_xS^{0,\pm1}$ ($x = 2$–5) clusters are marked in Fig. 6, and the details are summarized in Table 3. For $Au_2S^{0,\pm1}$ clusters, the Au–S bond length and the Au–S–Au bond angle in the Au_2S cluster are found to be 2.23 Å and 89.32°, using the PBE/aug-cc-pVTZ theory, respectively, and 2.25 Å and 94.48°, using the B3LYP/6-311++G(3df,3pd) theory, respectively. These results are in good agreement with the previously reported values, 2.25 Å and 87°.[2,35] They also may be compared to the results of Bagatur'yants[25] and Pérez's[64] 2.24 Å and 85.2° using the StR/E/CCSD(T) theory and 2.36 Å using the HF-MP2 theory, respectively.

Au_2S and its corresponding cationic cluster have similar lowest-energy structures. The Au–S bond length and the Au–S–Au bond angle in cationic Au_2S^+ are found to be 2.22 Å and 98.79°, respectively, using the PBE/aug-cc-pVTZ theory, and these values are in excellent agreement with those of a previous study[2] that used the GGA and LDA methods (2.23 Å and 98.5°, respectively). Unlike the Au_2S and Au_2S^+ clusters, Au_2S^- favors an asymmetric linear structure (S–Au–Au) according to the all employed methods, including the MP2, MP4, CCSD, and CCSD(T).[36] The Au–S bond lengths are found to be 2.24 Å and 2.27 Å using the PBE/aug-cc-pVTZ and the B3LYP/6-311++G(3df,3pd) theories, respectively.

For the lowest-energy isomers of all $Au_2S^{0,\pm1}$ species, the Au–S bond lengths are found to increase, while the Au–S–Au bond angle decreases, with the addition of one more electron (electric charge: +1, 0 and −1). The same trend is also observed in $Au_xS^{0,\pm1}$ ($x = 3$–5) clusters, while the general geometric change following electron removal is that the Au–S bond length is slightly shortened, and the Au–S–Au bond angle becomes wider.

The bond lengths of the lowest-energy isomers of $Au_xS^{0,\pm1}$ ($x = 1$–10) clusters are plotted in Fig. 7. In general, the bond length increases with the increasing no. of Au atoms. For smaller cationic Au_xS^+ clusters, the Au–S bond lengths are the smallest among the series of Au_xS clusters.

Table 3 Geometrical parameters ($r1$, $r2$, and $r3$ represent Au–S bond lengths in Å, and α represents the Au–S–Au bond angle) of the lowest-energy isomers of $Au_xS^{0,\pm1}$ ($x = 2$–5) clusters obtained using PBE/aug-cc-pVTZ (PBE), and B3LYP/6-311++G(3df,3pd) (B3LYP) theory

		Methods		
Species	Parameters	PBE	B3LYP	Calculated values
Au_2S^+	$r1$	2.22	2.24	2.23[a]
	α	98.79	101.89	98.5[a]
Au_2S	$r1$	2.23	2.25	2.25[b], 2.24[c], 2.36[e]
	α	89.32	94.48	87[b], 85.2[c]
Au_2S^-	$r1$	2.24	2.27	
Au_3S^+	$r1$	2.26	2.28	2.28[a]
	α	93.78	97.6	83.3[d]
Au_3S	$r1$	2.28	2.32	2.31[b], 2.37[e]
	α	80.36	96.54	75.34[e]
Au_3S^-	$r1$	2.4	2.41	
	$r2$	2.4	2.41	
	α	69.77	70.4	
Au_4S^+	$r1$	2.25	2.28	2.27[a]
	$r2$	2.22	2.24	
	α	99.26	102.75	
Au_4S	$r1$	2.27	2.29	2.29[b], 2.46[e]
	$r2$	2.26	2.29	
	α	88.2	90.1	
Au_4S^-	$r1$	2.35	2.37	
	$r2$	2.37	2.38	
	α	78.85	80.13	
Au_5S^+	$r1$	2.31	2.32	
	$r2$	2.32	3.15	3.21[a]
	$r3$	2.28	2.27	
	α	82.08	84.71	
Au_5S	$r1$	2.35	2.35	2.31[b], 2.46[e], 2.33[f]
	α	74.11	65.89	
Au_5S^-	$r1$	2.31	2.36	
	$r2$	2.31	2.36	
	α	81.53	81.35	

[a] Ref. 2: GGA, LDA. [b] Ref. 35: *ab initio* ultra-soft pseudopotential. [c] Ref. 25: StR/E/CCSD(T). [d] Ref. 53: MP2/11-VE/R. [e] Ref. 60: post HF/MP2. [f] Ref. 52: GGA-DFT/PW91PW91.

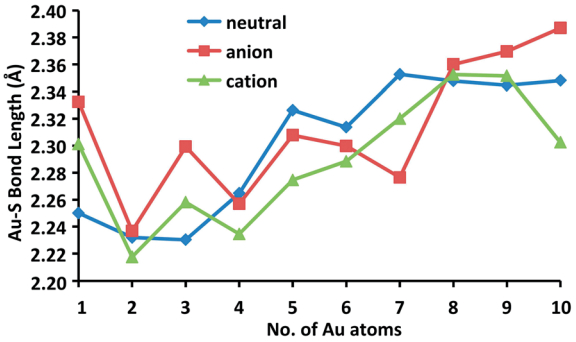

Fig. 7 Au–S bond lengths in Å of the lowest-energy isomers of $Au_xS^{0,\pm1}$ ($x = 1$–10) clusters obtained using B3LYP/6-311++G(3df,3pd) level of theory.

3.4. Relative stabilities of $Au_xS^{0,\pm1}$ species

To confirm the assumption stated above that anionic clusters may better used in catalysis, the stabilities of neutral clusters and their corresponding anionic and cationic clusters were compared based on their binding energies per atom (BE) and second-order differences in total energy (Δ^2E). The BE was calculated as follows:

$$\mathrm{BE}(\mathrm{Au}_n\mathrm{S}^-) = \frac{E(\mathrm{S}^-) + nE(\mathrm{Au}) - E(\mathrm{Au}_n\mathrm{S}^-)}{n+1}$$

$$\mathrm{BE}(\mathrm{Au}_n\mathrm{S}) = \frac{E(\mathrm{S}) + nE(\mathrm{Au}) - E(\mathrm{Au}_n\mathrm{S})}{n+1}$$

$$\mathrm{BE}(\mathrm{Au}_n\mathrm{S}^+) = \frac{E(\mathrm{S}^+) + nE(\mathrm{Au}) - E(\mathrm{Au}_n\mathrm{S}^+)}{n+1}$$

and Δ^2E is defined in the equations below:

$$\Delta^2E(\mathrm{Au}_n\mathrm{S}^-) = E(\mathrm{Au}_{n-1}\mathrm{S}^-) + E(\mathrm{Au}_{n+1}\mathrm{S}^-) - 2E(\mathrm{Au}_n\mathrm{S}^-)$$
$$\Delta^2E(\mathrm{Au}_n\mathrm{S}) = E(\mathrm{Au}_{n-1}\mathrm{S}) + E(\mathrm{Au}_{n+1}\mathrm{S}) - 2E(\mathrm{Au}_n\mathrm{S})$$
$$\Delta^2E(\mathrm{Au}_n\mathrm{S}^+) = E(\mathrm{Au}_{n-1}\mathrm{S}^+) + E(\mathrm{Au}_{n+1}\mathrm{S}^+) - 2E(\mathrm{Au}_n\mathrm{S}^+)$$

where E is the total energy of the system. The BE and Δ^2E of the lowest-energy configurations for $Au_xS^{0,\pm1}$ species are plotted in Fig. 8. The BE and Δ^2E are sensitive quantities that reflect the relative stabilities of the clusters.

As presented in Fig. 8a, with the successive addition of Au atoms, the BE value increases. It can be readily observed that the different charges lead to enormous changes in the structural stability of the $Au_xS^{0,\pm1}$ species. The average binding energies of the cationic clusters are significantly higher than those of the corresponding neutral and anionic clusters; the anionic clusters have the smallest BE values among these species. These results indicate that the removal of an electron can strengthen the stability of a neutral cluster.

For the cationic species, the BE (Fig. 8a) values are quite high for $x = 2$ and 3 and then exhibit a small dip at Au_4S^+, followed by a quite flat trend up to $x = 10$, except for a slight fluctuation at Au_9S^+. A visible peak appears at $x = 3$, which hints that Au_3S^+ is more stable than its neighboring clusters. The lowest-energy structure of the Au_3S^+ cluster is a 3D structure that possesses D_{3h} symmetry, which is the smallest 3D structure observed in this species.

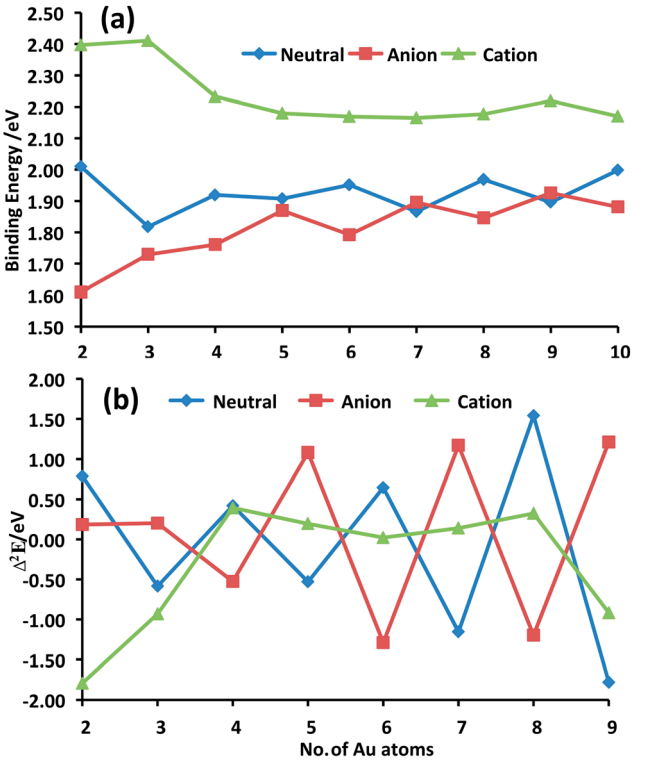

Fig. 8 Relative stabilities: binding energy (a) and second-order difference energies (b) for the lowest-energy structures of neutral and ionic Au_xS clusters with $x = 1$–10.

In contrast to the cationic species, the BE and Δ^2E exhibit an interesting, pronounced even-odd alternating behavior as a function of cluster size for the neutral and anionic species, which indicates that $Au_{3,5,7,9}S^-$ and neutral $Au_{2,4,6,8}S$ clusters have higher stability compared with their neighboring clusters. It is interesting to consider the enhanced stability for the Au_5S^- cluster that is due to a closed electron shell in a simple delocalized electron-shell model. That is, an anionic species with an even number of electrons is more stable than one with an odd number of electrons.

3.5. Electronic properties of $Au_xS^{0,\pm1}$ species

The electronic properties of $Au_xS^{0,\pm1}$ clusters can be described by using the energy difference between the highest occupied and lowest unoccupied molecular orbital (HOMO–LUMO) energy level, which reflects the ability for electrons to jump from HOMO to LUMO orbital and provides an important criterion for judging the stability of clusters. A large gap corresponds to a high strength required to perturb the electronic structure, namely a bigger gap indicates a weaker chemical activity. The calculated HOMO–LUMO gaps for the neutral and corresponding anionic and cationic clusters are presented in Fig. 9. One can find that the HOMO–LUMO gap represent a similar oscillating behaviors as observed for the BE and Δ^2E. The HOMO–LUMO gaps of neutral and anionic clusters exhibit an odd–even oscillatory behavior. That is, the clusters with odd number of atoms have an enhanced chemical stability. Moreover, it is worth pointing out that the largest HOMO–LUMO

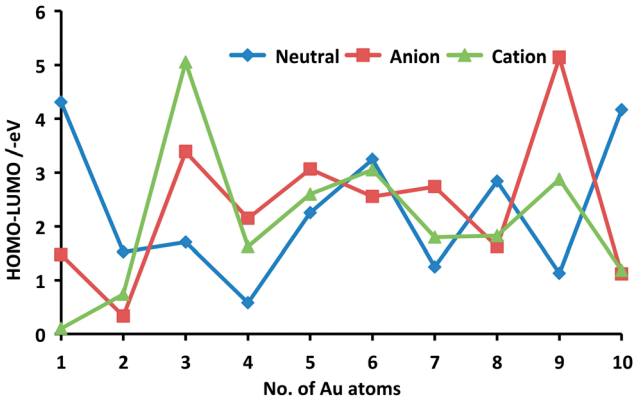

Fig. 9 Size dependence of the HOMO–LUMO gaps for the lowest-energy structure of $Au_xS^{0,\pm1}$ ($x = 1$–10) clusters.

energy gap for anionic Au_9S^- is found for the most stable configuration of the anionic clusters, and all the odd number of Au atoms keep higher stability compared with their neighboring clusters. For cationic species, Au_3S^+ cluster is the most stable one, which possessing the largest HOMO–LUMO gap among the whole cationic species. Compared with the electronic properties study of pure Au clusters,[68,72] incorporation of the S atom can increase or decrease the energy gap. The Au–S clusters at different electron charges have significantly difference in chemical stabilities and electronic properties.

4. Conclusions

We report herein a systematic theoretical study of Au_xS and the corresponding cationic and anionic clusters in several theoretical frameworks at different levels of approximation. We present a detailed investigation of the equilibrium atomic geometries, electronic structures, relative stabilities, and bonding characteristics of $Au_xS^{0,\pm1}$ ($x = 1$–10). The Au–S bond lengths are found to increase, while the Au–S–Au bond angles decrease, with the addition of one more electron (electric charge: +1, 0 and −1) for Au_xS, ($x = 2$–5). The same species with different electric charges possess different configurations. The lowest-energy structures of the cationic clusters are found to be 3D structures for sizes as small as $x = 3$, while for the Au_xS clusters, the 3D structures first manifest at a size of $x = 6$, and the 2D-to-3D crossover appears at a size of $x = 8$ for the Au_xS^- clusters. The tendency toward planarity of the Au–S clusters may be attributed to the strong relativistic effects of the Au atom and the similar electronegativity between the Au and S atoms. We may regard the Au_5S cluster as the building-block unit for the evolution of larger Au–S clusters. Of the $Au_xS^{0,\pm1}$ clusters, the anionic Au_xS^- clusters may be the most active species for catalysis.

Acknowledgements

The theoretical work was supported by grants from the National Natural Science Foundation of China (21073196, 21133008), Director Fund of AIOFM (Y23H161131 and Y03AG31146), Chinese Academy of Sciences. Acknowledgement is also made to the Thousand Youth Talents Plan.

References

1 Q. Sun, Q. Wang, B. K. Rao and P. Jena, *Phys. Rev. Lett.*, 2004, **93**, 186803.
2 H. Woldeghebriel and A. Kshirsagar, *J. Chem. Phys.*, 2007, **127**, 224708.
3 H. F. Qian and R. C. Jin, *Chem. Mater.*, 2011, **23**, 2209.
4 Y. Zhu, H. Qian, B. A. Drake and R. Jin, *Angew. Chem., Int. Ed.*, 2010, **49**, 1295.
5 Y. M. Liu, H. Tsunoyama, T. Akita and T. Tsukuda, *Chem. Commun.*, 2010, **46**, 550.
6 M. M. Maye, J. Luo, Y. H. Lin, M. H. Engelhard, M. Hepel and C. J. Zhong, *Langmuir*, 2003, **19**, 125.
7 C. Majumder, T. M. Briere, H. Mizuseki and Y. Kawazoe, *J. Chem. Phys.*, 2002, **117**, 2819.
8 R. Rousseau and D. Marx, *J. Chem. Phys.*, 2000, **112**, 761.
9 H. Häkkinen, R. N. Barnett and U. Landman, *Phys. Rev. Lett.*, 1999, **82**, 3264.
10 S. E. WallaceWilliams, C. A. James, S. deVries, M. Saraste, P. Lappalainen, J. vanderOost, M. Fabian, G. Palmer and W. H. Woodruff, *J. Am. Chem. Soc.*, 1996, **118**, 3986.
11 M. Dachraoui and J. Vedel, *Sol. Cells*, 1985, **15**, 319.
12 C. Zhang, B. Yoon and U. Landman, *J. Am. Chem. Soc.*, 2007, **129**, 2228.
13 A. A. Herzing, C. J. Kiely, A. F. Carley, P. Kandon and G. J. Hutchings, *Science*, 2008, **321**, 1331.
14 S. N. Rashkeev, A. R. Lupini, S. H. Overbury, S. J. Pennycook and S. T. Pantelides, *Phys. Rev. B: Condens. Matter Mater. Phys.*, 2007, **76**, 035438.
15 W. Huang and L. S. Wang, *Phys. Rev. Lett.*, 2009, **102**, 153401.
16 M. P. Johansson, A. Lechtken, D. Schooss, M. M. Kappes and F. Furche, *Phys. Rev. A: At., Mol., Opt. Phys.*, 2008, **77**, 053202.
17 E. M. Fernández, J. M. Soler, I. L. Garzón and L. C. Balbás, *Phys. Rev. B: Condens. Matter Mater. Phys.*, 2004, **70**, 165403.
18 H. M. Lee, M. F. Ge, B. R. Sahu, P. Tarakeshwar and K. S. Kim, *J. Phys. Chem. B*, 2003, **107**, 9994.
19 S. Gilb, P. Weis, F. Furche, R. Ahlrichs and M. M. Kappes, *J. Chem. Phys.*, 2002, **116**, 4094.
20 H. Häkkinen and U. Landman, *Phys. Rev. B: Condens. Matter Mater. Phys.*, 2000, **62**, 2287.
21 H. W. Ghebriel and A. Kshirsagar, *J. Chem. Phys.*, 2007, **126**, 244705.
22 I. P. Hamilton, *Chem. Phys. Lett.*, 2004, **390**, 517.
23 J. M. Seminario, C. E. De la Cruz and P. A. Derosa, *J. Am. Chem. Soc.*, 2001, **123**, 5616.
24 M. M. Jobbins, A. F. Raigoza and S. A. Kandel, *J. Phys. Chem. C*, 2011, **115**, 25437.
25 A. A. Bagatur'yants, A. A. Safonov, H. Stoll and H. J. Werner, *J. Chem. Phys.*, 1998, **109**, 3096.
26 Y. Wang, Q. Chi, J. Zhang, N. S. Hush, J. R. Reimers and J. Ulstrup, *J. Am. Chem. Soc.*, 2011, **133**, 14856.
27 H. Qian, M. Zhu, C. Gayathri, R. R. Gil and R. Jin, *ACS Nano*, 2011, **5**, 8935.
28 F. Tielens and E. Santos, *J. Phys. Chem. C*, 2010, **114**, 9444.
29 P. Maksymovych, O. Voznyy, D. B. Dougherty, D. C. Sorescu and J. T. Yates, *Prog. Surf. Sci.*, 2010, **85**, 206.

30 J. Gottschalck and B. Hammer, *J. Chem. Phys.*, 2002, **116**, 784.
31 I. L. Garzón, J. A. Reyes-Nava, J. I. Rodriguez-Hernández, I. Sigal, M. R. Beltrán and K. Michaelian, *Phys. Rev. B: Condens. Matter Mater. Phys.*, 2002, **66**, 073403.
32 D. Fujita, K. Ohnishi and T. Ohgi, *Sci. Technol. Adv. Mater.*, 2002, **3**, 283.
33 Y. Akinaga, T. Nakajima and K. Hirao, *J. Chem. Phys.*, 2001, **114**, 8555.
34 M. C. Leavy, S. Bhattacharyya, W. E. Cleland and C. L. Hussey, *Langmuir*, 1999, **15**, 6582.
35 C. Majumder and S. K. Kulshreshtha, *Phys. Rev. B: Condens. Matter Mater. Phys.*, 2006, **73**, 155427.
36 H. Wen, Y. R. Liu, T. Huang, K. M. Xu, W. J. Zhang, W. Huang and L. S. Wang, *J. Chem. Phys.*, 2013, **138**, 174303.
37 S. Bulusu, X. Li, L. S. Wang and X. C. Zeng, *Proc. Natl. Acad. Sci. U. S. A.*, 2006, **103**, 8326.
38 Q. Sun, B. V. Reddy, M. Marquez, P. Jena, C. Gonzalez and Q. Wang, *J. Phys. Chem. C*, 2007, **111**, 4.
39 W. Huang, M. Ji, C. D. Dong, X. Gu, L. M. Wang, X. G. Gong and L. S. Wang, *ACS Nano*, 2008, **2**, 897.
40 W. Huang, S. Bulusu, R. Pal, X. C. Zeng and L. S. Wang, *J. Chem. Phys.*, 2009, **131**, 234305.
41 W. Huang, A. P. Sergeeva, H. J. Zhai, B. B. Averkiev, L. S. Wang and A. I. Boldyrev, *Nat. Chem.*, 2010, **2**, 202.
42 W. Huang, R. Pal, L. M. Wang, X. C. Zeng and L. S. Wang, *J. Chem. Phys.*, 2010, **132**, 054305.
43 J. P. Perdew, K. Burke and M. Ernzerhof, *Phys. Rev. Lett.*, 1996, **77**, 3865.
44 B. Delley, *J. Chem. Phys.*, 1990, **92**, 508.
45 Y. L. Wang, X. B. Wang, X. P. Xing, F. Wei, J. Li and L. S. Wang, *J. Phys. Chem. A*, 2010, **114**, 11244.
46 X. Gu, S. Bulusu, X. Li, X. C. Zeng, J. Li, X. G. Gong and L. S. Wang, *J. Phys. Chem. C*, 2007, **111**, 8228.
47 A. D. Becke, *J. Chem. Phys.*, 1993, **98**, 5648.
48 C. T. Lee, W. T. Yang and R. G. Parr, *Phys. Rev. B: Condens. Matter Mater. Phys.*, 1988, **37**, 785.
49 K. A. Peterson and C. Puzzarini, *Theor. Chem. Acc.*, 2005, **114**, 283.
50 K. Raghavachari and G. W. Trucks, *J. Chem. Phys.*, 1989, **91**, 1062.
51 E. L. Bylaska, *et al.*, *NWCHEM. A computational chemistry package for parallel computers, version 5.1.1*, Pacific Northwest National Laboratory, Richland, WA 99352, USA. 2009.
52 C. Hampel, K. A. Peterson and H. J. Werner, *Chem. Phys. Lett.*, 1992, **190**, 1–12.
53 M. J. Frisch, M. Headgordon and J. A. Pople, *Chem. Phys. Lett.*, 1990, **166**, 275.
54 C. Majumder, A. K. Kandalam and P. Jena, *Phys. Rev. B: Condens. Matter Mater. Phys.*, 2006, **74**, 205437.
55 P. Pyykkö, K. Angermaier, B. Assmann and H. Schmidbaur, *J. Chem. Soc., Chem. Commun.*, 1995, **18**, 1889.
56 H. Häkkinen, B. Yoon, U. Landman, X. Li, H. J. Zhai and L. S. Wang, *J. Phys. Chem. A*, 2003, **107**, 6168.
57 F. Furche, R. Ahlrichs, P. Weis, C. Jacob, S. Gilb, T. Bierweiler and M. M. Kappes, *J. Chem. Phys.*, 2002, **117**, 6982.
58 H. Häkkinen, M. Moseler and U. Landman, *Phys. Rev. Lett.*, 2002, **89**, 033401.
59 B. Kiran, X. Li, H. J. Zhai and L. S. Wang, *J. Chem. Phys.*, 2006, **125**, 133204.
60 X. Li, B. Kiran and L. S. Wang, *J. Phys. Chem. A*, 2005, **109**, 4366.
61 B. Kiran, X. Li, H. J. Zhai, L. F. Cui and L. S. Wang, *Angew. Chem., Int. Ed.*, 2004, **43**, 2125.
62 H. J. Zhai, C. Q. Miao, S. D. Li and L. S. Wang, *J. Phys. Chem. A*, 2010, **114**, 12155.
63 H. J. Zhai, L. S. Wang, D. Y. Zubarev and A. I. Boldyrev, *J. Phys. Chem. A*, 2006, **110**, 1689.
64 G. Bravo-Pérez and I. L. Garzón, *J. Mol. Struct.: THEOCHEM*, 2002, **619**, 79.
65 L. M. Wang and L. S. Wang, *Nanoscale*, 2012, **4**, 4038.
66 P. Shao, X. Y. Kuang, Y. R. Zhao, Y. F. Li and S. J. Wang, *J. Mol. Model.*, 2012, **18**, 3553.
67 H. J. Zhai, C. Buergel, V. B. Koutecky and L. S. Wang, *J. Am. Chem. Soc.*, 2008, **130**, 9156.
68 C. J. Wang, X. Y. Kuang, H. Q. Wang, H. F. Li, J. B. Gu and J. Liu, *Comput. Theor. Chem.*, 2012, **1002**, 31.
69 R. B. Ross, J. M. Powers, T. Atashroo, W. C. Ermler, L. A. LaJohn and P. A. Christiansen, *J. Chem. Phys.*, 1990, **93**, 6654.
70 D. J. Wales and J. P. K. Doye, *J. Phys. Chem. A*, 1997, **101**, 5111.
71 S. Grimme, *J. Comput. Chem.*, 2004, **25**, 1463.
72 L. L. Yan, Y. R. Liu, T. Huang, S. Jiang, H. Wen, Y. B. Gai, W. J. Zhang and W. Huang, *J. Chem. Phys.*, 2013, **139**, 244312.